

Gravimetric and Density Functional Theory Investigations on 4-Aminoantipyrin Schiff Base as an Inhibitor for Mild Steel in HCl Solution

K. Mohsen Raheef¹, H. S. Qasim², A. A. Radhi², W. Kh. Al-Azzawi³, M. M. Hanoon², A. A. Al-Amiery^{4,5*}

¹ Ashur University College, P.O. Box: 10001, Baghdad, Iraq.

² Production and Metallurgy Engineering Department, University of Technology, P.O. Box: 10001, Baghdad, Iraq.

³ Department of Medical Instruments Engineering Techniques, Al-Farahidi University, P.O. Box: 10001, Baghdad, Iraq.

⁴ Department of Chemical and Process Engineering, Faculty of Engineering and Built Environment, Universiti Kebangsaan Malaysia, P.O. Box: 43600 UKM Bangi, Selangor, Malaysia.

⁵ Energy and Renewable Energies Technology Center, University of Technology-Iraq, P.O. Box: 10001, Baghdad, Iraq.

ARTICLE INFO

Article history:

Received: 26 Dec 2022

Final Revised: 17 Feb 2023

Accepted: 20 Feb 2023

Available online: 21 May 2023

Keywords:

Aminoantipyrine

Schiff base

Corrosion inhibitor

DFT

LUMO

ABSTRACT

Metal corrosion, in general, is a serious economic problem. One of the most effective ways to prevent corrosion on metal surfaces is to use corrosion inhibitors, especially green organics. Here, the effects of concentration, exposure time, and temperature on the antiproliferative ability of 4-aminoantipyrine derivative were investigated. The 4-aminoantipyrine derivative showed significant corrosion resistance to mild steel melting in a 1M hydrochloric acid environment, as observed from the weight loss method. At 303 K and a dose of 500 ppm, the maximum inhibitory efficacy of the 4-aminoantipyrine derivative was 96.1 %. Corrosion test results showed that the 4-aminoantipyrine derivative has an inhibitory effect of more than 88 % at the concentration of 400 ppm and inhibits corrosion through an adsorption mechanism. The inhibitory potency of the 4-aminoantipyrine derivative changed inversely with a long exposure time, while temperature affected it directly. The Langmuir model was used to control the physical and chemical adsorption of its 4-aminoantipyrine derivative as a corrosion inhibitor on metallic surfaces. Data from density functional theory simulations help bridge the gap between theoretical studies and experimental approaches. Prog. Color Colorants Coat. 16 (2023), 255-269© Institute for Color Science and Technology.

1. Introduction

Mild steel is a material that is widely used in various manufacturing and construction processes, including design and construction. Unfortunately, one of the major problems with using mild steel is the material's susceptibility to corrosion [1]. Corrosion in structural steel is a natural but manageable phenomenon. Inhibitors are important additives to protect structural steel from corrosion. Pickling is a typical industrial

cleaning process that removes scale and metal oxide deposits in oil drilling operations and petrochemical production. This process must be controlled as the mineral acids used are highly corrosive [2]. Organic molecules containing heteroatoms such as sulfur, oxygen, and nitrogen are effective corrosion inhibitors due to their ability to adsorb and inhibit active sites on metal substrates [3]. These organic inhibitors consist of two components, hydrophobic and hydrophilic, mostly

*Corresponding author: * dr.ahmed1975@gmail.com
dr.ahmed1975@ukm.edu.my

surfactants. Hydrophilic head groups (polar solvents) are usually ionizable and have a considerable affinity for water. Hydrophobic tails, on the other hand, are usually hydrocarbon (branched or linear). The head assembly can be attached to metal surfaces, forming a protective layer on the metal surface and protecting it from corrosion in acidic or corrosive liquids [4]. Environmentally friendly organic inhibitor technology has evolved in response to needs.

Despite their good efficiency, inorganic inhibitors (such as nitrate, chromate, phosphate, molybdate, etc.) are frequently used to prevent corrosion in structural alloys [5]. Theoretical chemical techniques are just as crucial as experimental techniques to identify corrosion inhibitors. Several quantum chemical factors can be used to interpret the activity of an inhibitor without the need for experimentation [6]. Quantitative chemical calculations can be used to produce materials that act as corrosion inhibitors between organic molecules. Atomic charges, molecular orbital energies, and energy are categories for the quantum chemical quantities often utilized in theoretical corrosion investigations [7]. In other words, it's important to determine corrosion inhibitor factors, including molecular activity, structure, and load. The molecule's potential structure may provide insight into the steric obstruction or how the inhibitor interacts with the metal solution interface. No studies have been reported on the 4-aminoantipyrene Schiff inhibitor used in this current study. This investigation aims to study the ability of the Schiff base "N-(4-amino-1,5-dimethyl-2-phenyl-1H-pyrazole-3 (2H)-ylidene)thiazol-2-amine" which is described in Figure 1 to the corrosion resistance of mild steel in 1 M hydrochloric acid solution using gravimetric techniques and DFT calculations.

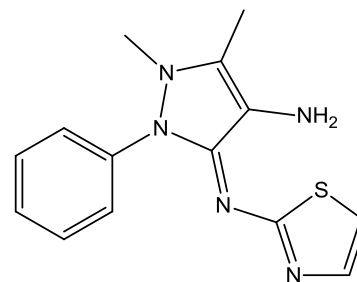


Figure 1: Molecular structure of (E)-N-(4-amino-1,5-dimethyl-2-phenyl-1H-pyrazole-3 (2H)-ylidene)thiazol-2-amine.

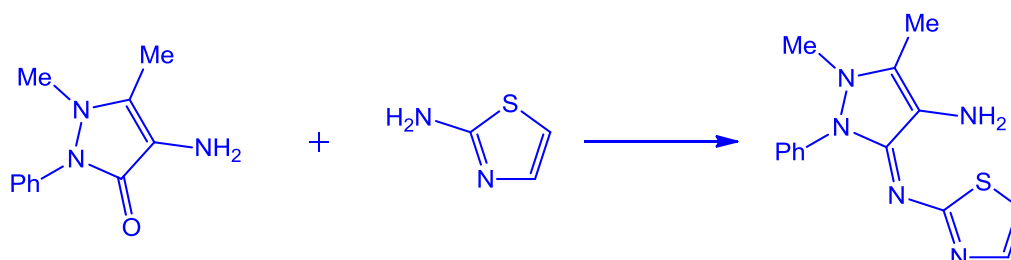
2. Experimental

2.1. Synthesis of testes inhibitor

The synthesis of the corrosion inhibitor was based on the reference [8]. Equal volumes of 2-aminothiazole and 4-aminoantipyrene were refluxed into a sufficient volume of ethyl alcohol for 5 h, and the product was filtered and recrystallized from ethyl alcohol. Scheme 1 represents the outline synthesis of the target compound. The yield was 71 %, and the melting point was 180 °C. Chemical Formula: $C_{14}H_{15}N_5S$. Micro elemental analysis: C, 58.92 %; H, 5.30 %; N, 24.54 % (Calculated), C, 50.01%; H, 5.27 %; N, 24.47 % (Found). Proton NMR: δ 2.11 (3H, s), 3.49 (3H, s), 6.61 (1H, d, $J=7.1$ Hz), 7.19-7.24 (3H, dd, $J=7.1$ Hz), 7.48-7.61 (3H, dd, $J=8.2, 7.9$ Hz), 7.59 (d, $J=3.2, 1.7$ Hz)).

2.2. Mild steel preparation

A section of mild steel with composition (wt. %) of 0.01 Al, 0.05 Mn, 0.05 S, 0.09 F, 0.21 C, 0.38 Si, balance iron. Tested metal coupons cut to size 25×20×0.3 mm were cleaned with silicon carbide paper of different grit from 320 to 1200. The cleaning process is based on ASTM G1-03 [8] technology.



Scheme 1: The synthesis of the tested corrosion inhibitor.

2.3. Hydrochloric acid solution

The hydrochloric acid solution was 1 M HCl with different exposure times (1, 5, 10, 24, and 48 hours). Different inhibitor concentrations were 0.0, 100, 200, 300, 400, 500, and 1000 ppm. The temperatures used were 303, 313, 323, and 333 K.

2.4. Weight loss techniques

The weight loss indicates the difference in mass of the sample before and after it is exposed to an acidic environment. It has been evaluated at different temperatures, periods, and concentrations. Based on the data obtained and the formula equation, the wear rate was determined depending on the weight loss [9]. The corrosion rate was calculated as follows in equation 1:

$$C_R(\text{mmpy}) = 87600W/a\rho t \quad (1)$$

Where, W is the weight loss of the mild steel coupon (mg), a is the mild steel coupon area (cm²), ρ is the mild steel coupon density (gcm⁻³), and t is the immersion period (hours).

The inhibition efficiency was determined according to equation 2:

$$IE\% = 1 - \frac{C_{R(\text{inh})}}{C_{R(\text{blank})}} \times 100 \quad (2)$$

where, C_{R(blank)} is the rate of corrosion of mild steel in the absence of the inhibitor, C_{R(inh)} is the rate of corrosion of mild steel in the presence of the inhibitor.

Based on equation 3, the surface coverage area (θ) was determined for various inhibitor concentrations in corrosive solution from the weight loss measurements.

$$\theta = 1 - \frac{C_{R(\text{inh})}}{C_{R(\text{blank})}} \quad (3)$$

2.5. Quantum chemical calculations

The theoretical chemistry calculations have been conducted through Gaussian 09 [10]. The inhibitor structure in the gas phase was optimized using the B3LYP method, and the basis was set to "6-31G++" (d,p). As per Koopman's theorem [11], the ionization potential (I) and electron affinity (A) relate to E_{HOMO} and E_{LUMO}, respectively and were calculated using Equations 4 and 5, respectively:

$$I = -E_{HOMO} \quad (4)$$

$$A = -E_{LUMO} \quad (5)$$

Equations 6 to 11 were used to determine the electronegativity (χ), softness (σ), and hardness (η):

$$\chi = \frac{I+A}{2} \quad (6)$$

$$\eta = \frac{I-A}{2} \quad (7)$$

$$\sigma \sim \eta^{-1} \quad (8)$$

Equation 9 was applied to calculate the fractional number of transported electrons (ΔN), [10]:

$$\Delta N = \frac{\chi_{Fe} - \chi_{inh}}{2(\eta_{Fe} + \eta_{inh})} \quad (9)$$

The electronegativity value for iron (χ_{Fe}) was equal to 7 eV, whereas the hardness of iron η_{Fe} was equal to 0 eV as in equation 10:

$$N = \frac{7 - \chi_{inh}}{2(\eta_{inh})} \quad (10)$$

3. Results and Discussion

3.1. Inhibitor concentration and exposure time effects

At 303 K, I ran exposures of 1, 5, 10, 24, and 48 hours. 4-aminoantipyrine derivatives were exposed to hydrochloric acid environments at different concentrations to assess their effectiveness as green corrosion inhibitors. Figure 2 presents the results of the exposure procedure. Figure 2 shows that the inhibition efficiency improves with immersion time (up to 24 h) at the same concentration. The corrosion rate slows with increasing immersion time above 24 hours. The shape of the protective layer begins to decrease due to prolonged contact with the hydrochloric acid solution, the longer the exposure time is greater than 24 hours. The increase in metallic substrate mass, which lowers as more corrosive ions attack the metallic substrate, shows that the rate of corrosion increases as more hydrogen protons are generated. The amino group in the heterocyclic ring allows the 4-aminoantipyrine derivative to react with iron and other metal cations. The iron derivative 4-aminoantipyrine is created when the amino group combines with the Fe³⁺ ion. By sticking to the metal surface, the 4-aminoantipyrine derivative will stop further corrosion.

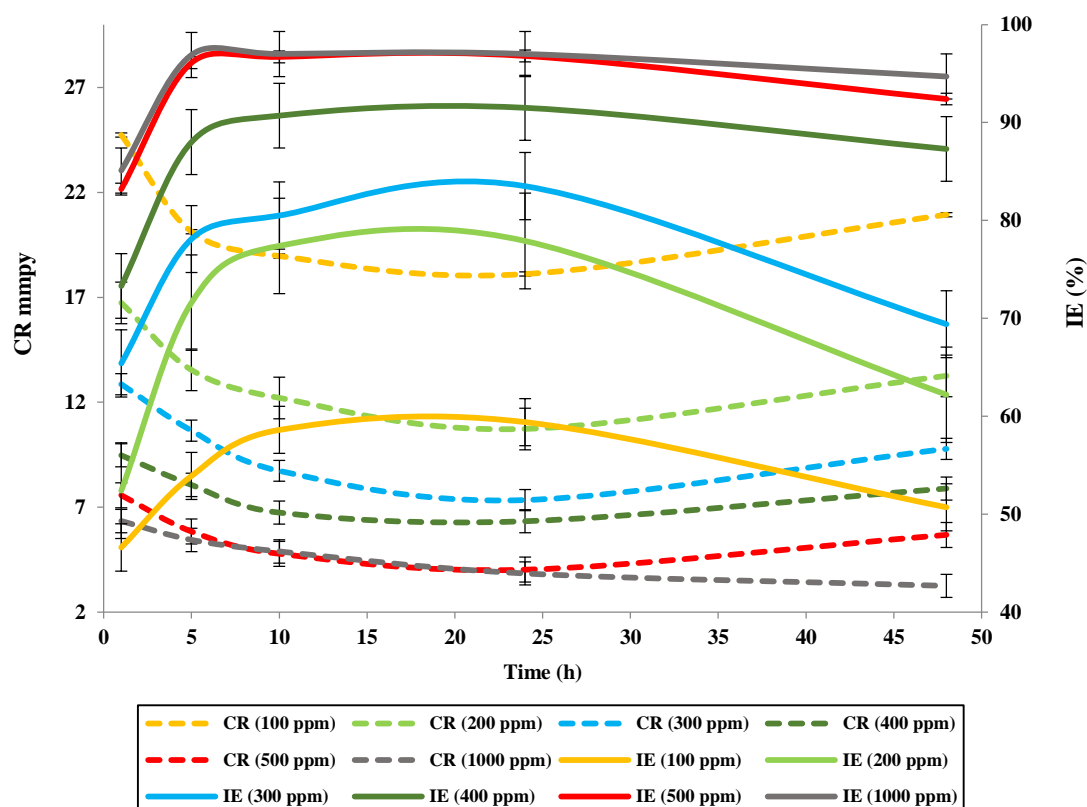


Figure 2: Exposure durations and inhibitor concentration against corrosion rate and inhibition efficiency at Temperature 303 K.

3.2. Temperature effects

Figure 3 displays the outcomes of the mass loss techniques computations together with inhibition efficiency values. Figure 3's study reveals how temperature affects inhibition effectiveness. As the HCl solution temperature rises, the inhibition's effectiveness decreases. The number of dissolving increases with temperature. Removing the inhibitor particles from the metal surface causes corrosion when the temperature rises. This event increases the surface area of mild steel in interface with the acidic environment and, in turn, increases the corrosion rate. In the presence of HCl, mild steel surface corrosion is followed by hydrogen gas generation. Because the complex molecule in the inhibitor solution adhering to the surface of mild steel to produce a protective barrier that can block corrosion attacks, the addition of inhibitor concentration can increase efficiency. The mild steel surface will adsorb the 4-aminoantipyrine derivative to a greater extent at higher concentrations, boosting the inhibitor's ability to prevent corrosion.

3.3. Adsorption isotherms

The degree of interaction between molecules of different inhibitors and the metal surface is explained by adsorption isotherms since the formation of protective films on metal surfaces resulted from molecules that have been adsorbed during organic corrosion inhibitors. It was determined that the inhibitory mechanism is adsorption using isotherm equations. Additionally, applying empirical equations like exponential, hyperbolic, logarithmic, and power to the known processes of the adsorption process is challenging to get the closest equation that connects the concentration of inhibitors to the adsorbed concentration at saturation. In addition to being straightforward, the Frumkin, Langmuir, and Temkin isotherms make it simple to use their parameters to characterize the corrosion inhibition system. [22].

Isotherm models are typically represented using equation 11 [23].

$$f(\theta, \chi) \exp(-a\theta) = KC \quad (11)$$

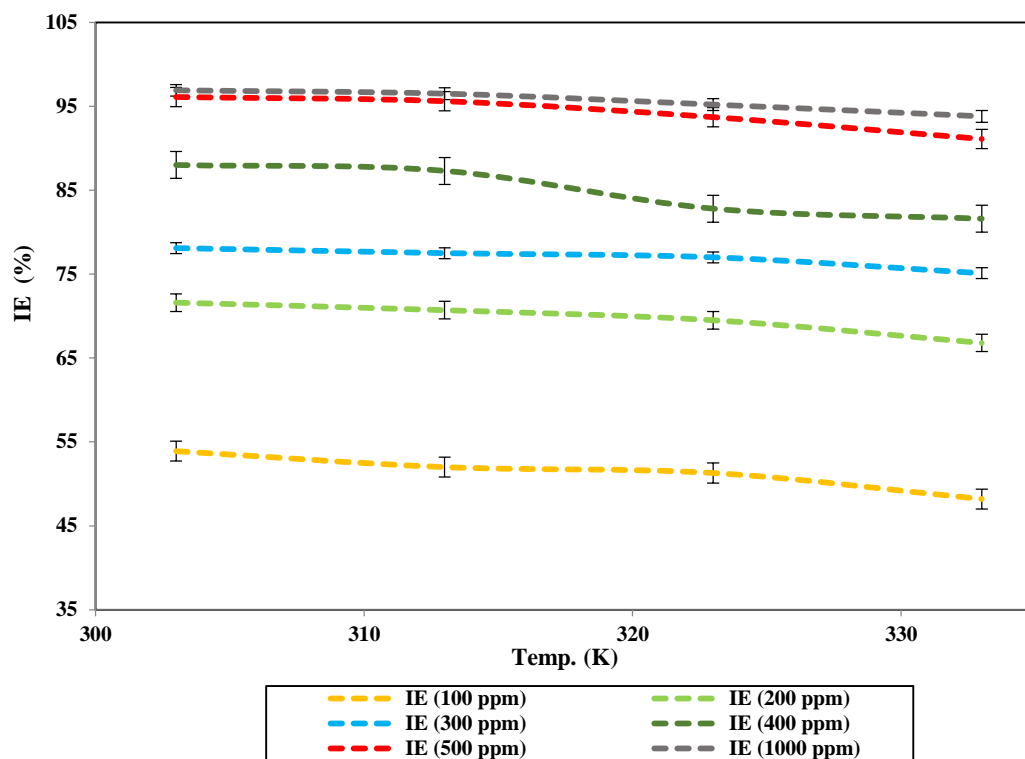


Figure 3: Temperature and inhibitor concentrations against inhibition efficiency for exposure duration 5h.

Adsorption of particles onto the metallic surface always occurs in conjunction with the inhibitory mechanism [23]. Equation 3 was used to determine the percentage of the surface covered at any given time. The following isotherms were looked into for a proper understanding of the mechanism involved.

3.3.1. Langmuir model

The Langmuir isotherm is described by equation 12. K_{ads} is the adsorption-desorption constant, and θ is the surface coverage

$$\frac{C}{\theta} = \frac{1}{K_{ads}} + C \quad (12)$$

3.3.2. Frumkin model

The linear version of the Frumkin isotherm is represented by equation 13.

$$\log \frac{\theta}{1-\theta} = 2.303 \log k + 2\alpha\theta \quad (13)$$

3.3.3. Tempkin model

Equation 14 relates the concentration (C) of inhibition to the amount of surface coverage (θ). Constant K and

parameter (α) for the Tempkin isotherm at various temperatures and times were determined from Eq. 14 after linearization using the logarithmic transformation 14.

$$\log \frac{\theta}{C} = \log k + \alpha\theta \quad (14)$$

The conclusion drawn from the different isotherms was sufficient to describe the 4-aminoantipyrin derivative molecules' adsorption process and inhibitory ability at the interface between the corrosive environment and mild steel. The following isotherm plots' calculations provide significant findings: Due to significant R2 values and a slope that was near 1, Freundlich, Langmuir, and Temkin measurements at various temperatures showed that the process of 4-aminoantipyrin derivative adsorption on mild steel surfaces followed the Langmuir isotherm at all temperatures examined. According to the Langmuir equation, this suggests that the 4-aminoantipyrin derivative molecules are evenly distributed in monolayers on the surface of mild steel [25].

Figure 4's Langmuir isotherm plot, which depicts the K_{ads} value as a straight line between $\log (C/\theta)$

and C_{inh} , was used to make this determination. The greater the adsorption and the more effective the inhibition, the higher the K_{ads} value, which measures how well an inhibitor molecule sticks to a metallic substrate [26]. The inhibitor that was tested had the highest K_{ads} value, suggesting that mild steel surfaces would be the best for adsorption. Equation 15 shows a relationship between the K_{ads} values and the common free energy of adsorption (ΔG_{ads}^0) determined by the relationship [27]:

$$\Delta G_{ads}^0 = -RT \ln(55.5K_{ads}) \quad (15)$$

When ΔG_{ads}^0 becomes less than 20 kJ mol^{-1} , physical adsorption occurs between charges on inhibitor molecules and the mild steel surface. When ΔG_{ads}^0 is greater than 40 kJ mol^{-1} , chemisorption occurs when unpaired electrons from the inhibitor molecules' heteroatoms transfer to the Fe-orbital on the metal surface to form a stable complex [28]. The ΔG_{ads}^0

was $37.85 \text{ kJ mol}^{-1}$. This investigation demonstrates a broad range of adsorption (involving both physisorption and chemisorption). Chemisorbed molecules are anticipated to provide more effective shielding because they reduce the metal's inherent reactivity at the spots where they are linked. Thus, it is difficult to discriminate between chemisorption and physisorption using just the ΔG_{ads}^0 value. In addition, inhibitors' physical adsorption on the metal surface takes place before their chemical adsorption [29].

3.4. DFT calculations

Quantum chemical simulations were carried out to examine the structural factors that affect the inhibition efficacy of inhibitors. The inhibitor's geometric and electrical structure was computed by maximizing its bond length. Figure 5 shows the optimal molecular structure with the lowest energy discovered using DFT computations.

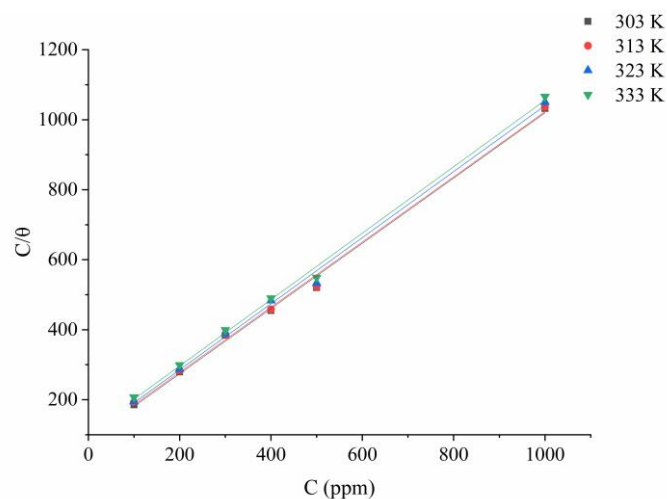


Figure 4: Langmuir isotherm models in treated solution at various temperature.

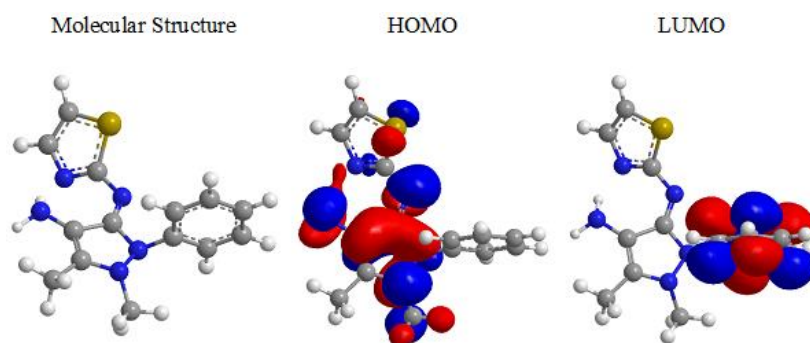


Figure 5: The neutral inhibitor at the optimal molecular structure, HOMO and LUMO, as determined by DFT/B3LYP/6-31G(d).

The following computations are used to determine quantum chemical variables: the highest occupied molecular orbital energy (EHOMO), the lowest-occupied molecular orbital energy (ELUMO), energy gap (ΔE), dipole moment (μ), electronegativity (χ), electron affinity (A), global hardness (η), softness (σ), ionization potential (I), the total energy (TE) and the fraction of electrons transferred from the inhibitor to mild steel surface (ΔN). These parameters are determined and presented in Table 1.

High values of EHOMO are likely to suggest a propensity of the molecule to donate electrons to suitable acceptor molecules with low energy and vacant molecular orbitals. The energy of HOMO is frequently related to the ability of a molecule to give electrons. As a result, the energy of the LUMO signal denotes the molecule's capacity to receive electrons [12, 13]. Therefore, the likelihood that the molecule will receive electrons increases with decreasing ELUMO values. With rising HOMO and falling LUMO energy values, the inhibitor's ability to attach to the metal surface increases. According to the calculations, the tested inhibitor had the lowest LUMO level or -1.113 eV, and the highest HOMO level, or -5.599 eV, which explained why increased HOMO and decreased LUMO energies are responsible for the highest inhibitory efficacy evaluated. The obtained results perfectly agree with the DFT simulation, which indicates that the evaluated inhibitor has significant inhibition potency. According to the study 4, the density for the tested inhibitor, HOMO, is primarily dispersed throughout the heterocyclic ring of 4-aminoantipyrine. The 4-aminoantipyrine's benzene ring is where the LUMO density is primarily concentrated.

The schematic diagram of frontier molecular orbitals for the tested inhibitor to its estimated energy gap, E, is shown in Figure 6. Corrosion inhibition is typically understood as the result of inhibitor molecules adhering to the metal surface. Two adsorption modes are conceivable. The interaction of electrically charged metal surfaces and charged species in most solutions is necessary for physical adsorption. The chemisorption mode implies charge sharing from the inhibitor molecule to the open orbitals of the metal with low energy. The effectiveness of the tested inhibitors and adsorption

parameters as a function of temperature revealed that the physisorption phenomena is more preferred [15, 16]. Therefore, in the study, the tested inhibitor effectively prevented mild steel from corroding in 1 M HCl. The evaluated inhibitor is regarded as a noteworthy effective inhibitor. According to the data, the tested inhibitor had a greater ΔE_{gap} . This parameter measures the stability of the generated complex on the metal surface. The stability of the produced complex is higher the lower the value of ΔE_{gap} . The tested inhibitor's ΔE_{gap} value is -4.486 eV. The relationship between ΔE_{gap} and inhibition effectiveness is frequently highlighted in the literature as well. According to our theoretical findings, there is no connection between inhibitory effectiveness and ΔE_{gap} .

Also estimated was the number of electrons transported (ΔN). The values of (ΔN) revealed that Lukovits' study [17] agreed with the inhibitory efficiency of electron donation. The capacity of this inhibitor to give electrons to the metal surface is great, and if N 3.6, the inhibition efficiency rises by increasing the ability to donate electrons to the metal surface. The absolute value of ΔN may not reflect reality, but it does represent tendencies within a collection of molecules. The number of electrons that leave the donor and enter the acceptor molecule is not perfectly represented by the ΔN value.

Table 1: The 4-aminoantipyrine Schiff base theoretical parameters.

Quantum Chemical Parameters	Values
E_{HOMO} (eV)	-5.5999
E_{LUMO} (eV)	-1.113
ΔE_{gap}	-4.486
μ (Debye)	4.9834
χ	3.356
I	5.599
A	1.113
η	2.243
Σ	0.4458
ΔN	0.8123

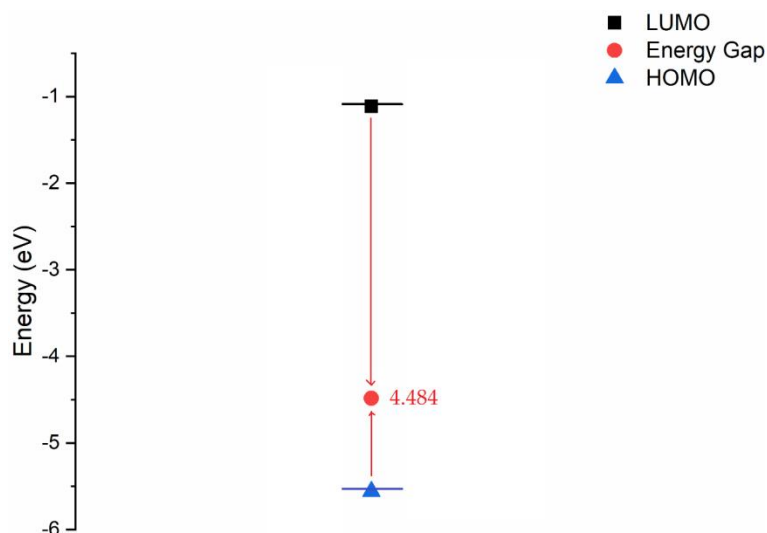


Figure 6: Frontier molecular orbital correlation diagram for the evaluated inhibitor.

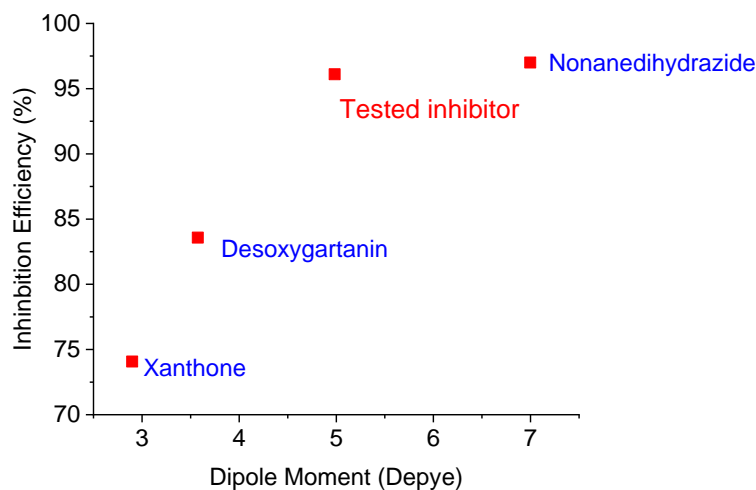


Figure 7: The relationship between the inhibitory performances and the dipole moments.

On the other hand, the molecule's dipole moment is the most frequently used parameter to explain polarity [18]. A covalently bonded bond's dipole moment serves as a measurement for its polarity. Its formula is the sum of the charges on the atoms and the separation of the two bound atoms. However, the total dipole moment only captures the overall polarity of a molecule. The vector sum of the individual bond dipole moments can be used to approximate the overall molecular dipole moment for a whole molecule. Theoretical research has demonstrated a strong correlation between the dipole moment and the effectiveness of the inhibition (Figure 7). Indeed, as the

dipole moment increases, the inhibition efficiency increase [19-21].

3.5. Inhibition mechanism

Organic molecules adsorb on the surface of steel to prevent corrosion. Nitrogen, oxygen, and the fused benzene ring are present in the 4-aminoantipyrine Schiff base molecules. It has been found that chemisorption and physisorption processes account for the majority of inhibitor adsorption on metallic substrate surfaces. Through donor-acceptor interactions with the empty Fe-orbitals, 4-aminoantipyrine Schiff base molecules are adsorbed onto the mild steel surface. The inhibitor's

nitrogen and oxygen atoms can transfer one pair of electrons to the unoccupied d-orbitals of the metal, forming a coordinating contact. In addition, the metal atom can make the same type of bond with the electrons of the aromatic rings. As shown in Figure 8, the metallic substrate/corrosive solution interface may have a potential blockage of the adsorption inhibitor molecules' process. Additionally, the d-orbitals of the iron atoms receive the free electrons from the nitrogen and oxygen atoms.

3.6. Comparison study

Table 2 demonstrates that the tested inhibitor N-(4-amino-1,5-dimethyl-2-phenyl-1H-pyrazole-3 (2H)-ylidene) thiazol-2-amine was a one-shot synthesis, has a substantial inhibiting efficiency when matched to several other produced inhibitors. The corrosion inhibitors in Table 2 were much more expensive to synthesize than the studied inhibitor because their

protective effectiveness was proportionately lower or comparable, requiring numerous stages and expensive solvents.

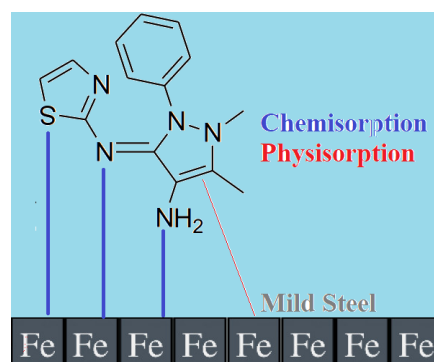


Figure 8: The proposed protected inhibited mechanism for the metallic substrate by Physisorption and Chemisorption methods.

Table 2: Compares the investigational inhibitor to verified steel inhibitors in hydrochloric acid solution.

Corrosion inhibition	Nature of adsorption	Alloy	Verified steel inhibitors	Ref.
96.1 %	Physisorption & chemisorption	Mild steel		-
91 %	Physisorption and chemisorption	Mild steel		[30]
98 %	Physisorption and chemisorption	Mild steel		[31]
94 %	Physisorption and chemisorption	Mild steel		[31]
96 %	Physisorption and chemisorption	Mild steel		[32]

Table 2: Continue.

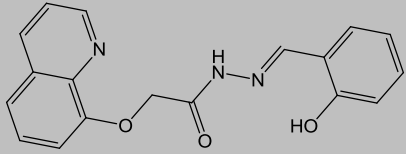
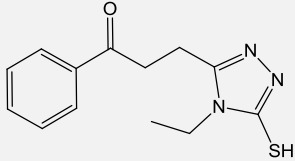
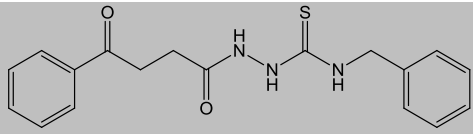
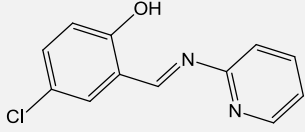
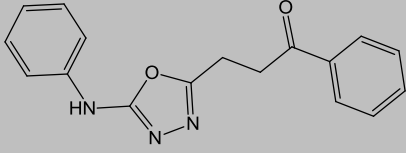
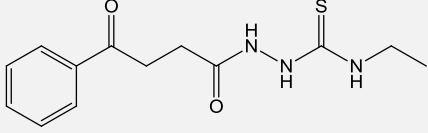
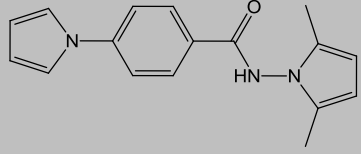
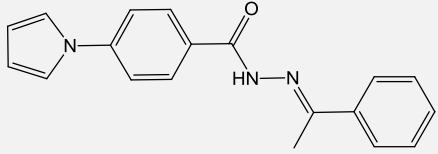
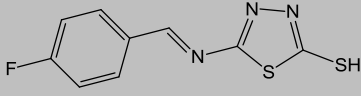
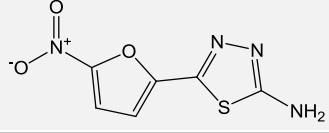
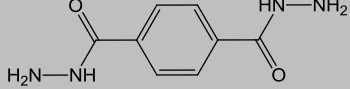
Corrosion inhibition	Nature of adsorption	Alloy	Verified steel inhibitors	Ref.
93%	Physisorption and chemisorption	Mild steel		[33]
97%	Physisorption and chemisorption	Mild steel		[34]
92%	Physisorption and chemisorption	Mild steel		[35]
91%	Physisorption and chemisorption	C. steel		[36]
95%	Physisorption and chemisorption	Mild steel		[37]
96%	Physisorption and chemisorption	Mild steel		[38]
95%	Physisorption and chemisorption	Mild steel		[39]
94%	Physisorption and chemisorption	Mild steel		[40]
91%	Physisorption and chemisorption	Mild steel		[41]
83%	Physisorption and chemisorption	Mild steel		[42]
96%	Physisorption and chemisorption	Mild steel		[43]

Table 2: Continue.

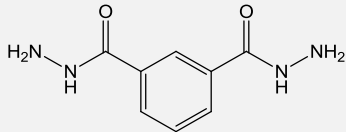
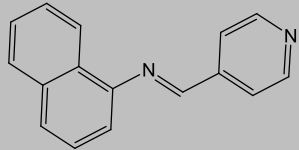
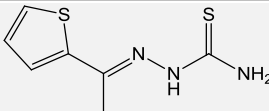
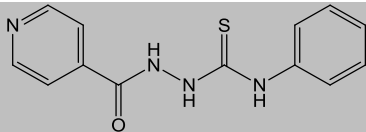
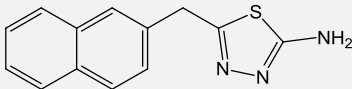
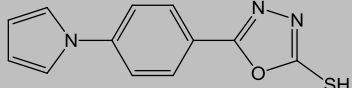
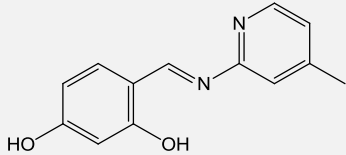
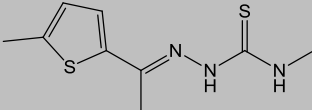
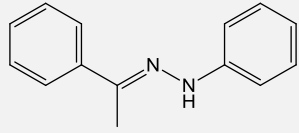
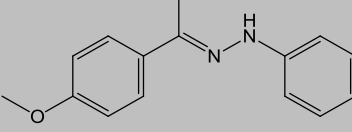
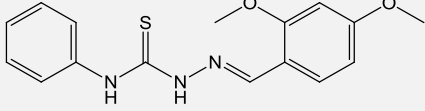
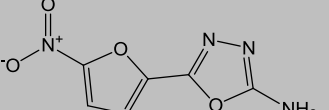
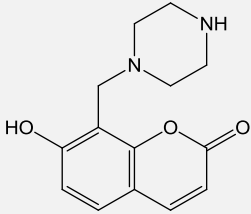
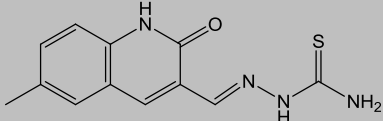
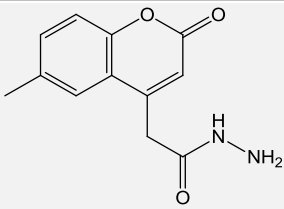
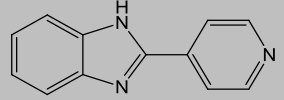
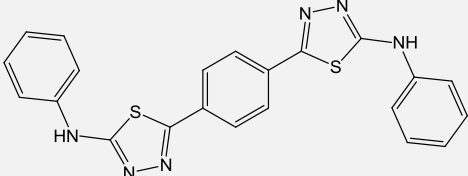
Corrosion inhibition	Nature of adsorption	Alloy	Verified steel inhibitors	Ref.
97 %	Physisorption and chemisorption	Mild steel		[44]
91 %	Physisorption and chemisorption	Mild steel		[45]
96 %	Physisorption and chemisorption	Mild steel		[46]
96 %	Physisorption and chemisorption	Mild steel		[47]
95 %	Physisorption and chemisorption	C. steel		[48]
95 %	Physisorption and chemisorption	Mild steel		[49]
93 %	Physisorption and chemisorption	C. steel		[50]
95 %	Physisorption and chemisorption	Mild steel		[51]
83 %	Physisorption and chemisorption	Mild steel		[52]
95 %	Physisorption and chemisorption	Mild steel		[53]
94 %	Physisorption and chemisorption	Mild steel		[54]
79 %	Physisorption and chemisorption	Mild steel		[55]

Table 2: Continue.

Corrosion inhibition	Nature of adsorption	Alloy	Verified steel inhibitors	Ref.
93 %	Physisorption and chemisorption	Mild steel		[56]
95 %	Physisorption and chemisorption	Mild steel		[57]
94 %	Physisorption and chemisorption	Mild steel		[58]
93 %	Physisorption and chemisorption	Mild steel		[59]
94 %	Physisorption and chemisorption	Mild steel		[59]

4. Conclusions

The current study aimed to assess the 4-aminoantipyrine Schiff base's effectiveness in inhibiting the corrosion of mild steel in hydrochloric acid solutions. Furthermore, to determine the effectiveness of the inhibition, the adsorption characteristics of the mild steel were investigated using weight loss methods. This event led to

the classification of 4-aminoantipyrine Schiff base as a potent inhibitor with a promising inhibition efficiency of 96.1 %. The 4-aminoantipyrine Schiff base's chemical composition provided mild steel protection through physisorption and chemisorption. These findings were in agreement with the DFT used in this investigation.

5. References

1. G. E. Badr, The role of some thiosemicarbazide derivatives as corrosion inhibitors for C-steel in acidic media, *Corros. Sci.*, 51(2009), 2529-2536.
2. M. Goyal, S. Kumar, I. Bahadur, C. Verma, E. Ebenso, Organic corrosion inhibitors for industrial cleaning of ferrous and non-ferrous metals in acidic solutions: A review, *J. Mol. Liq.*, 256(2018), 565-573.
3. S. Ghareba, S. Omanovic, Interaction of 12-aminododecanoic acid with a carbon steel surface: towards the development of 'green' corrosion inhibitors, *Corros. Sci.*, 52(2010), 2104-2113.
4. A. Yıldırım, M. Cetin, Synthesis and evaluation of new long alkyl side chain acetamide, isoxazolidine and isoxazoline derivatives as corrosion inhibitors, *Corros. Sci.*, 50(2008), 155-165.
5. S. K. Saha, A. Dutta, P. Ghosh, D. Sukul, P. Banerjee, P. Novel Schiff-base molecules as efficient corrosion inhibitors for mild steel surface in 1 M HCl medium: experimental and theoretical approach, *Phys. Chem. Chem. Phys.*, 18(2016), 17898-17911.
6. X. Li, S. Deng, H. Fu, Three pyrazine derivatives as corrosion inhibitors for steel in 1.0 M H₂SO₄ solution,

- Corros. Sci.*, 53(2011), 3241-3247.
7. M. Karelson, V. Lobanov, A. Katritzky Quantum-chemical descriptors in QSAR/QSPR studies, *Chem. Rev.*, 96(1996), 1027-1044.
 8. J. Kumaran, S. Priya, J. Gowsika, N. Jayachandramani, S. Mahalakshmi, Synthesis, spectroscopic characterization, in silico DNA studies and antibacterial activities of Copper(II) and Zinc(II) complexes derived from thiazole based pyrazolone derivatives, *Res. J. Pharm. Biol. Chem. Sci.*, 4(2013), 279-288.
 9. A.S.T.M. Standard, Standard practice for preparing, cleaning, and evaluating corrosion test specimens, American Society for Testing and Materials G1-03, (2011).
 10. Gaussian 09, Revision D.01, M. J. Frisch, G. W. Trucks, H. B. Schlegel, G. E. Scuseria, M. A. Robb, J. R. Cheeseman, G. Scalmani, V. Barone, B. Mennucci, G. A. Petersson, H. Nakatsuji, M. Caricato, X. Li, H. P. Hratchian, A. F. Izmaylov, J. Bloino, G. Zheng, J. L. Sonnenberg, M. Hada, M. Ehara, K. Toyota, R. Fukuda, J. Hasegawa, M. Ishida, T. Nakajima, Y. Honda, O. Kitao, H. Nakai, T. Vreven, J. A. Montgomery, Jr., J. E. Peralta, F. Ogliaro, M. Bearpark, J. J. Heyd, E. Brothers, K. N. Kudin, V. N. Staroverov, R. Kobayashi, J. Normand, K. Raghavachari, A. Rendell, J. C. Burant, S. S. Iyengar, J. Tomasi, M. Cossi, N. Rega, J. M. Millam, M. Klene, J. E. Knox, J. B. Cross, V. Bakken, C. Adamo, J. Jaramillo, R. Gomperts, R. E. Stratmann, O. Yazyev, A. J. Austin, R. Cammi, C. Pomelli, J. W. Ochterski, R. L. Martin, K. Morokuma, V. G. Zakrzewski, G. A. Voth, P. Salvador, J. J. Dannenberg, S. Dapprich, A. D. Daniels, Ö. Farkas, J. B. Foresman, J. V. Ortiz, J. Cioslowski, and D. J. Fox, Gaussian, Inc., Wallingford CT, (2009).
 11. T. Koopmans, Ordering of wave functions and eigenenergies to the individual electrons of an atom, *Physica*, 1(1933), 104-113.
 12. L. Larabi, Y. Harek, O. Benali, S. Ghalem, Hydrazide derivatives as corrosion inhibitors for mild steel in 1 M HCl, *Prog. Org. Coat.*, 54(2005), 256-263.
 13. Lukovits, E. Kálmán, F. Zucchi, Corrosion inhibitors-correlation between electronic structure and efficiency, *Corrosion*, 57(2001), 3-12.
 14. A. Zarrouk, A. Dafali, B. Hammouti, H. Zarrok, S. Boukhris, M. Zertoubi, Synthesis, characterization and comparative study of functionalized quinoxaline derivatives towards corrosion of copper in nitric acid medium, *Int. J. Electrochem. Sci.*, 5(2010), 46-53.
 15. A. Fiala, A. Chibani, A. Darchen, A. Boulkamh, K. Djebbar, Investigations of the inhibition of copper corrosion in nitric acid solutions by ketene dithioacetal derivatives, *Appl. Surf. Sci.*, 253(2007), 9347.
 16. M. M. El-Naggar, Bis-aminoazoles corrosion inhibitors for copper in 40 M HNO₃ solutions, *Corros. Sci.*, 42(2000), 773.
 17. Lukovits, E. Kálmán, F. Zucchi, Corrosion inhibitors-correlation between electronic structure and efficiency, *Corrosion*, 57(2001), 11-23.
 18. O. Kikuchi, Systematic QSAR procedures with quantum chemical descriptors, *Quant. Struct.-Act. Relat.*, 6(1987), 179.
 19. K. Al-Azawi, S. Al-Baghdadi, A. Mohamed, A. Al-Amiery, T. Abed, S. Mohammed, A. Kadhum, A. Mohamad, Synthesis, inhibition effects and quantum chemical studies of a novel coumarin derivative on the corrosion of mild steel in a hydrochloric acid solution, *Chem. Central J.*, 10(2016), 1-9.
 20. A. Al-Amiery, A. Mohamad, A. Kadhum, I. Shaker, W. Isahak, M. Takriff, Experimental and theoretical study on the corrosion inhibition of mild steel by nonanedioic acid derivative in hydrochloric acid solution, *Sci. Rep.*, 12(2022), 1-21.
 21. F. Ramadhani, E. Emriadi, S. Syukri, Theoretical study of xanthone derivative corrosion inhibitors using density functional theory (DFT), *J. Kimia Valensi*, 6(2020), 96-105.
 22. A. Singh, M. Quraishi, Effect of cefazolin on the corrosion of mild steel in HCl solution, *Corros. Sci.*, 52(2010), 152-160.
 23. M. Ameer E. Khamis G. Al-Senani, Adsorption studies of the effect of thiosemicarbazides on the corrosion of steel in phosphoric acid, *Adsorpt. Sci. Technol.*, 8(2000), 177-194.
 24. A. Yaro A. Khadom, R. Wael, Apricot juice as green corrosion inhibitor of mild steel in phosphoric acid, *Alexandria Eng. J.*, 52(2013), 129-135.
 25. B. Meroufel O. Benali M. Benyahia Y. Benmoussa M. Zenasni, Adsorptive removal of anionic dye from aqueous solutions by algerian kaolin: characteristics, isotherm, kinetic and thermodynamic studies, *J. Mater. Environ. Sci.*, 3(2013), 482-491.
 26. I. Ahamad, R. Prasad, M. Quraishi, Inhibition of mild steel corrosion in acid solution by Pheniramine drug: Experimental and theoretical study, *Corr. Sci.*, 52(2010), 3033-3041.
 27. N. Kıcıır, G. Tansuğ, M. Erbil, T. Tüken. Investigation of ammonium (2, 4-dimethylphenyl)-dithiocarbamate as a new, effective corrosion inhibitor for mild steel, *Corr. Sci.*, 105(2016), 88-99.
 28. W. Li, Q. He, S. Zhang, C. Pei, B. Hou, Some new triazole derivatives as inhibitors for mild steel corrosion in acidic medium, *J. Appl. Electrochem.*, 38(2008), 289-295.
 29. S. Zhang, Z. Tao, S. Liao, F. Wu, Substitutional adsorption isotherms and corrosion inhibitive properties of some oxadiazol-triazole derivative in acidic solution, *Corr. Sci.*, 52(2010), 3126-3132.
 30. A. Alamiery, Study of corrosion behavior of N'-(2-(2-oxomethylpyrrol-1-yl) ethyl) piperidine for mild steel in the acid environment, *Biointerface Res. Appl. Chem.*, 12(2022), 3638-3646.
 31. A. Alamiery, A. Mohamad, A. Kadhum, S. Takriff, Comparative data on corrosion protection of mild steel in HCl using two new thiazoles, *Data in Brief*, 40(2022), 107838.
 32. A. M. Mustafa, F.F. Sayyid, N. Betti, L.M. shaker,

- M. M. Hanoon, A.A. Alamiery, A.A.H. Kadhum, M.S. Takriff, Inhibition of mild steel corrosion in hydrochloric acid environment by 1-amino-2-mercapto-5-(4-(pyrrol-1-yl)phenyl)-1,3,4-triazole, *South African J. Chem. Eng.*, 39(2022), 42-51.
33. A. Alamiery, Investigations on corrosion inhibitory effect of newly quinoline derivative on mild steel in HCl solution complemented with antibacterial studies, *Biointerface Res. Appl. Chem.*, 12(2022), 1561-1568.
34. A. Aziz, I.A. Annon, M. Abdulkareem, M. Hanoon, M. Alkaabi, L. Shaker, A. Alamiery, W. Wan Isahak, M. Takriff, Insights into corrosion inhibition behavior of a 5-Mercapto-1, 2, 4-triazole derivative for mild steel in hydrochloric acid solution: experimental and DFT studies, *Lubricants*, 9(2021), 122.
35. A. Alamiery, W. Isahak, M. Takriff, Inhibition of mild steel corrosion by 4-benzyl-1-(4-oxo-4-phenylbutanoyl)thiosemicarbazide: gravimetric, adsorption and theoretical studies, *Lubricants*, 9(2021), 93.
36. M.A. Dawood, Z.M.K. Alasady, M.S. Abdulazeez, D.S. Ahmed, G.M. Sulaiman, A.A.H. Kadhum, L.M. Shaker and A.A. Alamiery, The corrosion inhibition effect of a pyridine derivative for low carbon steel in 1 M HCl medium: Complemented with antibacterial studies, *Int. J. Corros. Scale Inhib.*, 10(2021), 1766-1782.
37. A. Alamiery, Corrosion inhibition effect of 2-N-phenylamino-5-(3-phenyl-3-oxo-1-propyl)-1,3,4-oxadiazole on mild steel in 1 M hydrochloric acid medium: Insight from gravimetric and DFT investigations, *Mater. Sci. Energy Technol.*, 4(2021), 398-406.
38. A. Alamiery, Short report of mild steel corrosion in 0.5 M H₂SO₄ by 4-ethyl-1-(4-oxo-4-phenylbutanoyl) thiosemicarbazide, *J. Tribologi*, 30(2021), 90-99.
39. A. Alamiery, Anticorrosion effect of thiosemicarbazide derivative on mild steel in 1 M hydrochloric acid and 0.5 M sulfuric Acid: Gravimetric and theoretical studies, *Mater. Sci. Energy Technol.*, 4(2021), 263-273.
40. A. Alamiery, W., Isahak, H. Aljibori, H. Al-Asadi, A. Kadhum, Effect of the structure, immersion time and temperature on the corrosion inhibition of 4-pyrrol-1-yl-n-(2,5-dimethyl-pyrrol-1-yl)benzoylamine in 1.0 M HCl solution, *Int. J. Corros. Scale Inhib.*, 10(2021), 700-713.
41. A. Alamiery, E. Mahmoudi and T. Allami, Corrosion inhibition of low-carbon steel in hydrochloric acid environment using a Schiff base derived from pyrrole: gravimetric and computational studies, *Int. J. Corros. Scale Inhib.*, 10(2021), 749-765.
42. A.J.M. Eltmimi, A. Alamiery, A.J. Allami, R.M. Yusop, A.H. Kadhum, T. Allami, Inhibitive effects of a novel efficient Schiff base on mild steel in hydrochloric acid environment, *Int. J. Corros. Scale Inhib.*, 10(2021), 634-648.
43. A. Alamiery, L. Shaker, A. Allami, A. Kadhum, M. Takriff, A study of acidic corrosion behavior of Furan Derived schiff base for mild steel in hydrochloric acid environment: Experimental, and surface investigation, *Mate. Today: Proceedings*, 44(2021), 2337-2341.
44. S. Al-Baghdadi, A. Al-Amiery, T. Gaaz, A. Kadhum, Terephthalohydrazide and isophthalo-hydrazide as new corrosion inhibitors for mild steel in hydrochloric acid: Experimental and theoretical approaches, *Koroze Ochrana Materialu*, 65(2021), 12-22.
45. M. Hanoon, A. Resen, L. Shaker, A. Kadhum, A. Al-Amiery, Corrosion investigation of mild steel in aqueous hydrochloric acid environment using n-(Naphthalen-1yl)-1-(4-pyridinyl)methanimine complemented with antibacterial studies, *Biointerface Res. Appl. Chem.*, 11(2021), 9735-9743.
46. S. Al-Baghdadi, T. Gaaz, A. Al-Adili, A. Al-Amiery, M. Takriff, Experimental studies on corrosion inhibition performance of acetylthiophene thiosemicarbazone for mild steel in HCl complemented with DFT investigation, *Intern. J. Low-Carbon Technol.*, 16(2021), 181-188.
47. A. Al-Amiery, Anti-corrosion performance of 2-isonicotinoyl-n-phenylhydrazinecarbothioamide for mild steel hydrochloric acid solution: Insights from experimental measurements and quantum chemical calculations, *Surface Rev. Letters*, 28(2021), 2050058.
48. M.S. Abdulazeez, Z.S. Abdullahe, M.A. Dawood, Z.K. Handel, R.I. Mahmood, S. Osamah, A.H. Kadhum, L.M. Shaker, A.A. Al-Amiery, Corrosion inhibition of low carbon steel in HCl medium using a thiadiazole derivative: weight loss, DFT studies and antibacterial studies, *Int. J. Corros. Scale Inhib.*, 10(2021), 1812-1828.
49. A. Mustafa, F. Sayyid, N. Betti, M. Hanoon, A. Al-Amiery, A. Kadhum, M. Takriff, Inhibition evaluation of 5-(4-(1H-pyrrol-1-yl)phenyl)-2-mercapto-1,3,4-oxadiazole for the corrosion of mild steel in an acidic environment: thermodynamic and DFT aspects, *Tribologia-Finnish J. Tribol.*, 38(2021), 39-47.
50. Y.M. Abdulsahib, A.J.M. Eltmimi, S.A. Alhabeeb, M.M. Hanoon, A.A. Al-Amiery, T. Allami, A.A.H. Kadhum, Experimental and theoretical investigations on the inhibition efficiency of N-(2,4-dihydroxytoluene)ylidene)-4-methylpyridin-2-amine for the corrosion of mild steel in hydrochloric acid, *Int. J. Corros. Scale Inhib.*, 10(2021), 885-899.
51. A. Khudhair, A. Mustafa, M. Hanoon, A. Al-Amiery, L. Shaker, T. Gazz, A. Mohamad, A. Kadhum, M. Takriff, Experimental and theoretical investigation on the corrosion inhibitor potential of N-MEH for mild steel in HCl, *Prog. Color Colorants Coat.*, 15(2021), 111-122.
52. D. Zinad, R. Salim, N. Betti, L. Shaker, A. AL-Amiery, Comparative investigations of the corrosion inhibition efficiency of a 1-phenyl-2-(1-phenylethylidene)hydrazine and its analog against mild steel corrosion in hydrochloric acid solution, *Prog. Color Colorants Coat.*, 15(2021), 53-63
53. R. Salim, N. Betti, M. Hanoon, A., Al-Amiery, 2-(2,4-Dimethoxybenzylidene)-N-

- phenylhydrazinecarbothioamide as an efficient corrosion inhibitor for mild steel in acidic environment, *Prog. Color Colorants Coat.*, 15(2021), 45-52.
54. A. Al-Amiery, L. Shaker, A.M. Takriff, Exploration of furan derivative for application as corrosion inhibitor for mild steel in hydrochloric acid solution: Effect of immersion time and temperature on efficiency, *Mater. Today: Proc.*, 42(2021), 2968-2973.
55. A.M. Resen, M.M. Hanoon, W.K. Alani, A. Kadhim, A.A. Mohammed, T.S. Gaaz4, A.A.H. Kadhum, A.A. Al-Amiery, M.S. Takriff, Exploration of 8-piperazine-1-ylmethylumbelliferone for application as a corrosion inhibitor for mild steel in hydrochloric acid solution, *Int. J. Corros. Scale Inhib.*, 10(2021), 368-387.
56. M. Hanoon, A., Resen, A. Al-Amiery, A. Kadhum, T. Takriff, Theoretical and experimental studies on the corrosion inhibition potentials of 2-((6-Methyl-2-ketoquinolin-3-yl)Methylene) hydrazinecarbothioamide for mild steel in 1 M HCl, *Prog. Color Colorants Coat.*, 15(2021), 21-33.
57. F. Hashim, T. Salman, S. Al-Baghdadi, T. Gaaz, A. Al-Amiery, Inhibition effect of hydrazine-derived coumarin on a mild steel surface in hydrochloric acid, *Tribologia*, , 37(2020), 45–53
58. A.M. Resen, M. Hanoon, R.D. Salim, A.A. Al-Amiery, L.M. Shaker, A.A.H. Kadhum, Gravimetric, theoretical, and surface morphological investigations of corrosion inhibition effect of 4-(benzoimidazole-2-yl) pyridine on mild steel in hydrochloric acid, *Koroze Ochrana Materialu*, 64(2020), 122-130.
59. A. Salman, Q. Jawad, K. Ridah, L. Shaker, A. Al-Amiery, Selected BIS-Thiadiazole: synthesis and corrosion inhibition studies on mild steel in HCl environment, *Surf. Rev. Lett.*, 27(2020), 2050014

How to cite this article:

K. Mohsen Raheef, H. S. Qasim, A. A. Radhi, W. Kh. Al-Azzawi, M. M. Hanoon, A. A. Al-Amiery, Gravimetric and Density Functional Theory Investigations on 4-Amioantipyrin Schiff Base as an Inhibitor for Mild Steel in HCl Solution. *Prog. Color Colorants Coat.*, 16 (2023), 255-269.

